Adaptation of the TLM method for sea radar application and simulation

Thibaut Lurton, Christophe Sintes, Michel Ney, René Garello

Adaptation of the TLM Method for Sea Radar Application and Simulation

Thibaut Lurton, Christophe Sintès, Michel M. Ney, and René Garello,
Telecom Bretagne, ITI Department, CNRS UMR 3192 LabSTICC/CID,
Technopôle Brest-Iroise, CS 83818 – 29238 Brest, France.

***Abstract*—This paper presents the adaptation of the Transmission-Line Matrix (TLM) electromagnetic simulation method to the case of the propagation of a radar electromagnetic signal over a sea water patch. The TLM is a full-wave and numerical method; in order to gain computation time, it is combined with ray-tracing in our approach. We propose an overview of the advantages and disadvantages of the use of the TLM method for the electromagnetic simulation of a radar observation. Then, we give details about the implementation of the TLM to model the interaction between an impinging electromagnetic wave and the ocean surface; this includes some particular modifications of the classical TLM technique, and a combination with spectral sea surface rendition methods. Using our simulation method and the radar equation, normalised cross sections can be derived and compared with models. Alternatively, some imagery process can be carried out on small areas using the synthetic aperture technique. Since virtually any sea/radar configuration can be explored, including the presence of manufactured objects in the midst of the simulated sea patch, the flexibility of our simulation tool is demonstrated.**

I. Introduction

Radar imaging of the sea surface is still a matter of active research, for various reasons. First, it is common knowledge that imaging land by means of radar is well mastered. However, there are still some issues to be addressed in the maritime domain: the process of synthetic aperture, for instance, is strongly affected by the movement of the sea. This has some important impact on the observation of sea surface that finds direct applications in many fields, such as geophysics (study of sea state, steepness of waves, roughness, currents, winds, etc.), environmental matters (e.g. pollution tracking), military purposes, civilian maritime surveillance, etc.

For all those applications, theoretical approaches can be of utmost significance in order to master the behaviour of radar signals in a maritime context.

As a sea surface is rough, it is not easy to derive an analytical solution to an electromagnetic wave propagation over it [1], [2]. Though other approaches are possible, in this article we focus on two types of methods: ray-tracing simulation and a numerical technique. Both will have their advantages and drawbacks: whilst the ray-tracing is fast, a numerical method requires a fair amount of computational time; on the other hand, the accuracy is much higher with a numerical approach than with ray-tracing, especially when small details—such as wavelets on a sea surface—are to be depicted.

The application of numerical methods to the simulation of radar propagation has already been explored under various forms. We can cite the Method of Moments as presented in [3], [4], [5], [6], [7], [8] and the Finite-Difference Time-Domain method as published in [9], [10], [11], [12], [13], [14], [15] for various configurations (1-D or 2-D rough surfaces, possible inclusion of an object, and different boundary conditions). Ray-tracing or plane-wave methods on the other hand have been widely explored and have simple theoretical basics.

Concerning the numerical technique used, we prefer the Transmission-Line Matrix (TLM) method, for reasons that shall be enlightened later. Like FDTD, TLM can be applied to arbitrary geometry and, since calculations are performed in the time domain, it allows one to process wide band signals. However, TLM is less dispersive and the condensed nature of the cell allows the computation of all field components at the same space location and time. Moreover, to the best of our knowledge, this method has not been applied to a radar simulation yet, which confers a certain prospective interest to this work.

The approach we propose consists in the combination of two types of simulation techniques, taking advantage of each method. Locally, i.e. in the vicinity of the sea surface which can be arbitrarily irregular, the problem will be addressed numerically, whilst a plane wave approach will be retained for the major part of the propagation where no obstacle is encountered since we are dealing with free space. Thus, we will limit the accurate numerical computation to the bare minimum needed in space, and rely on a plane wave approach for the rest of the simulation domain in order to reduce computational time.

In a first part of this paper, we will go through an overview of the structure of our simulation program, with in particular some details on the method used to combine a plane wave approach with a numerical technique, and a description of the approach used to model a sea surface in a numerical mesh. Finally, results will be presented and commented, with a discussion upon the efficiency of the method.

The following section exposes the underlying principles of the hybrid simulation technique we propose.

II. A PROPOSED HYBRID METHOD FOR RADAR PROPAGATION SIMULATION

A. Choice of technique and simulation principles

The difficulty to model radar propagation stems from two constraints: first, large distances are at stake, which excludes the possibility to directly use a numerical method; then, the shortness of the wavelength entails a good precision over the simulation, which cannot be reached through a sheer geometrical approach. Hence the idea to combine the two types of methods to build an effective tool.

On the one hand, plane waves are used to model the propagation of the radar wave through the large zone of free space between the radar and the sea surface. The plane wave approach we use in this study uses a simple ray-tracing technique, with no reflection involved. Fields are cast from the emission point to any point of the numerical computation zone using a basic propagation equation.

On the other hand, we use a numerical technique. The necessity of a numerical method to model the interaction between a radar wave and the sea surface stems from the need of a high degree of accuracy in the depiction of the phenomena at stake. As a matter of fact, the reflection of the radar wave on the sea surface will be resulting from small-scale phenomena such as Bragg scattering. A useful rule of thumb is to consider that the main contribution to the backscattering will be the effect of sea waves whose size is comparable to the main electromagnetic wavelength used. Due to the level of detail induced for high radar frequencies, it is not possible to rely on a simple ray-tracing process, and analytical solutions [1], [2] are cumbersome. We chose to use the TLM (Transmission-Line Matrix) method, for reasons discussed below.

Utilising a full-wave method such as the TLM is relevant first because it allows one to have access to the exact response of the impinging electromagnetic signal over a given sea patch. This way we can expect to compute thorough backscattered time signals. Then the TLM shows the advantage of the freedom of numerical modelling: no constraint is encountered as for the geometry, or physical and electromagnetic properties of the propagation medium. In the considered research field of simulations over a sea surface, we can expect a TLM mesh to handle virtually any kind of surface, with for instance no assumption on the degree of roughness, which is a limiting parameter of the analytical methods. It is also very easy to implement an object within the sea scene modelled, even of complex shape and of arbitrary electromagnetic characteristics.

A very interesting property of the TLM method for our concern is that it is well adapted to high permittivity contrasts as explained above. As the relative permittivity of sea water can be estimated around several dozens, versus a unit value for air, the high contrast configuration is wholly in the scope of the study.

As the TLM calculates the E- and H-field values at the same points of space and at the same temporal steps, the linking of the TLM computation with a plane wave approach is easier than it would have been with the common use of the FDTD scheme, which operates with half-step time and space shifts. Moreover, this is also an asset when an interface between two media of different electromagnetic characteristics is at stake and has to be depicted thoroughly, which is the case in this study.

Concerning computer costs, the TLM remains (like all volumic methods) a quite expensive method, with computational times directly proportional to the size of the scene modelled and the time iteration number considered. Our study was carried out with codes written in Fortran; nevertheless, adapting the code in C showed a significant gain in time. Likewise, the prospected adaptation of the algorithm in parallel computing makes it a promising and attractive numerical method.

As a conclusion, we can point out assets to the TLM method: first, as a full-wave method, it computes in the time-domain the exact behaviour of the electromagnetic signal when encountering the sea surface, and therefore yields thorough backscattering results. Compared to the FDTD, the TLM requires more variables per cell but it is less dispersive and computes all field components at the same time and position whilst keeping the same order of constraints on spatial discretisation. Its robustness in modelling complex structures such as PML has been demonstrated, along with its capacity to use variable meshing. Moreover, its adaptability to high permittivity contrast configurations makes it very suitable in presence of air/water interfaces. Concerning its linking with a plane wave approach, it is better suited than the FDTD because of the condensed character of the TLM node. In terms of resources, the long computation times are still a drawback, but should be reduced in the near future. These considerations are our main arguments for the use of the TLM method in our study.

Our method proceeds at different levels of space: at the sub-wavelength level, we deal with *TLM nodes* (the precise variety of which in this study being the *Symmetrical Condensed Nodes*, *SCN*), which as explained above can be seen as adjacent cubic cells. Their side is defined as being at most $\lambda/10$ (λ being the carrier electromagnetic wavelength in the medium), and each of the cells shows six facets that we shall refer to as *micro-facets*. Defining a spatial array of TLM nodes produces a whole mesh of cells; this is the actual zone over which the whole TLM computation and therefore the numerical part of the electromagnetic propagation simulation is carried out. In this 3-D zone, we shall implement the air/sea interface to be investigated. As one can see and as shown on Fig. 1, due to the geometry of the underlying TLM nodes, this interface will be "Manhattan"-modelled, i.e. it will stand as an arrangement of orthogonal micro-facets. The size of the TLM node, which is well below the wavelength of the incident electromagnetic wave, ensures that such a representation is viable. This rendition of the sea surface, encompassed in the total set of TLM nodes, will be referred to as a *patch*; its size will typically be of several electromagnetic wavelengths, and the ray-tracing operation will be led on these objects. Finally, at a higher level, a gathering of patches shall produce a whole

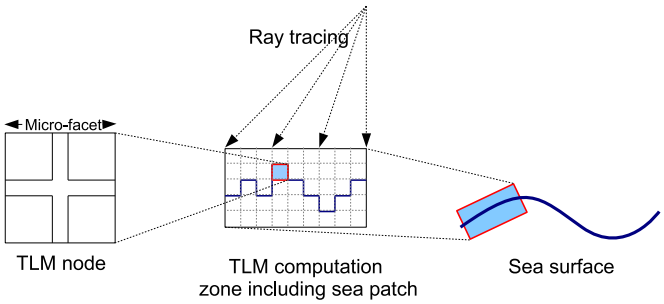

Figure 1. Overall view of the simulation principles, with terminology.

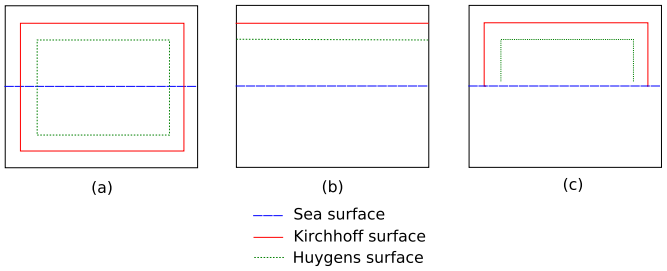

Figure 2. Different possible geometries for the Huygens and Kirchhoff surfaces. (a) Regular parallelepipeds; (b) planar surfaces; (c) bell-shaped surfaces.

sea surface. Passing from a ray-tracing/TLM computation over a series of single patches to data concerning a large area of sea can be carried out by statistical means, as detailed in section III-D. An overview of the whole set-up is presented in Fig. 1.

The following two paragraphs explain how the junction between ray-tracing and TLM computation is made, i.e. how fields cast upon the numerical computation zone are taken into account in the TLM algorithm, and how the backscattered signal is calculated from the TLM zone back to the emission point.

B. Use of the Huygens surface

The Huygens surface is a virtual closed surface in the TLM computation mesh whose role is to inject external source field values within the computational space. Its principles stem from the equivalent surface theorem, which states the equivalence of representation between imposing currents over a closed surface and setting outside field values to zero. In the downward propagation, from the radar to the sea patch, our simulation scheme uses a simple ray propagation technique: field values in the TLM mesh are computed taking into account the shape of the emitted time pulse and the position of the point considered, and assuming a spherical propagation of the electromagnetic wave. Given a sufficiently large distance between the emission point and the TLM computational space, it can reasonably be considered as a plane wave approach led by ray theory. This field-casting calculation is used to initialise electromagnetic values within the TLM zone. All TLM nodes are not concerned by this operation: the data initialisation is limited to a closed surface, the Huygens surface, on the sides of which the fields are cast and thus represent the feeding values for the TLM algorithm.

The basic requirement for the Huygens surface is for it to be a closed surface. In a first approach, we will simply consider it to be a parallelepiped.

C. Use of the Kirchhoff surface

In the upward part of the radar propagation, i.e. from the sea patch back to the emission point, the transformation is more complex and relies on the Kirchhoff integral. This expression links the field values taken on the sides of another virtual closed surface—the Kirchhoff surface—to the resulting electromagnetic components in any point of space, be it in far or near field. Using this computation, one can retrieve the electromagnetic field radiated back at the source point using values within the numerical computation space.

Any composant ψ of the electromagnetic field outside the Kirchhoff frontier can be calculated at a position $\vec{x}$ [16]:

$$\psi(\vec{x}) = -\frac{1}{4\pi}\iint_{S_1}\frac{e^{ikR}}{R}\vec{n'}\cdot\left[\vec{\nabla}'\psi(\vec{x'}) + ik\left(1+\frac{i}{kR}\right)\frac{\vec{R}}{R}\psi(\vec{x'})\right]dS'$$

For the sake of consistency, the Kirchhoff surface must strictly encompass the Huygens surface. Moreover, both surfaces must be closed, and the Kirchhoff surface must contain every radiating source. In our study, though, we relied on simplified schemes because difficulties arose due to the extension of the sea surface. Considering a virtually infinite surface in both horizontal dimensions, and assuming that the Huygens and Kirchhoff surfaces surround the air/water interface, it is contradictory to have a closed Kirchhoff surface encompassing the radiating elements (i.e. the water): the sea surface is necessarily intersected by the Kirchhoff surface, leaving a portion of sea outside the integration domain. We therefore chose to use planar horizontal Kirchhoff and Huygens surfaces, considering that they were approximations of closed surfaces of infinite extent. A comparison of the use of planar surfaces versus ideal closed surfaces was carried out and showed a sufficiently good concordance between the two to permit the approximation [17]. For the case of grazing angles, we can also use bell-shaped surfaces, which are more likely to take propagation under small angles into consideration. This is illustrated in figure 2.

D. Use of Perfectly Matched Layers

Because the individual patches the computation is performed on are finite in space, we must address the issue of truncated space: this is carried out in a classical way, using Bérenger's Perfectly Matched Layers (PMLs) [18]. These zones surround the computation space and consist in a certain number of cell layers with specific electromagnetic properties simulating an exponential decay of any outgoing wave. Typically, for our matter, a PML layer will have a depth of 15 cells, which ensures a quasi-total attenuation of outgoing signals.

E. Practical use

Most radar observations use the pulse compression technique to combine a fine range precision with a performing signal-to-noise ratio. This technique is based on the sending of long, frequency-modulated "chirp" signals instead of short pulses. The main drawback in trying to numerically model a signal such as a chirp is its cumbersome length, which induces a high number of TLM runs and therefore a long overall computation time.

We propose to utilise a shorter, equivalent signal in the simulation. Given the fact that matched filtering is a linear operation, we can admit that sending the whole chirp and performing the corresponding correlation on the simulated output signal is equivalent to sending directly the signal corresponding to the auto-correlated chirp. We remind that the range resolution gain that can be reached is $T\Delta f$ with T the length of the emitted signal and Δf the frequency band swept by the modulation. Thus the same gain can be applied to the length of the signal sent. Therefore, we use the already distance-resolved signal as input of the simulation; we will consider this signal as being shaped by a sinc function of argument $\pi\Delta f t\Lambda(t/T)$, Λ being the triangle function of domain $[-\frac{1}{2};\frac{1}{2}]$ and of unit amplitude. The time-resolved signal used as the simulation input will be composed of a sinusoid of frequency f_0 shaped by the first lobe of the function just mentioned.

The limits of such a model are the supposed characteristics of the propagation medium: we assume that it is non-dispersive. Taking the dispersion phenomenon into account was not envisaged in this study due to the cumbersome implementation of the related numerical procedures, involving convolution products of temporal sequences. The process however does exist [19], and the TLM method can handle dispersion in a general case. This can be added to the potentiality of the proposed scheme, though it was not explored in this first stage of the implementation.

This is for the sake of coherence with a real radar illumination using a chirp. We may now argue that, as far as the radar cross section is concerned, since it only depends on the frequency, the polarisation and target properties, any waveform shall in fact yield a consistent radar cross section within the frequency band considered. Therefore, we will use very simple signals to perform our RCS simulation, e.g. a few sinusoid arches at the centre frequency shaped in amplitude by a Gaussian envelope.

III. Adapting the TLM method to the observation of a sea patch

A. Sea surface representation

One of the key points in our backscattering modelling is the rendition of the sea surface. As said before, the main contribution to the backscattering of the electromagnetic wave by the water will be that of the surface waves of comparable size to the radar wavelength. It is thus necessary to have a fine mesh resolution; indeed, the upper limit of $\frac{\lambda_{min}}{10}$ for the spatial step fulfils the condition.

Spectral models used to generate a sea surface were empirically derived from in situ measurements, taking into account parameters such as wind speed, wind direction and fetch. Several propositions of spectra were enunciated [20], [21], [22], [23], [24], [25]. The latter (Elfouhaily's spectrum) was retained for its recent publication, its completeness, and the widespread use of it. This spectrum is particularly relevant because it covers all wave numbers, allowing the modelling of sea patches of any size.

Elfouhaily's spectrum is the combination of two sub-spectra on complementary frequency bands. Its expression can be found in [25].

Given this spectral expression, one can synthesise sea surfaces of any size, with the spatial resolution wanted, and under practically any wind conditions. One shall bear in mind that Elfouhaily's spectrum does not model phenomena such as wave breaking or white horses. Therefore, it is only realistic up to a certain wind speed. It is commonly accepted that Beaufort 3–4, which converts to a 10 kn, 20 km.h^{-1} or 6 m.s^{-1} wind speed, is a fair limit to wave breaking. Nonetheless, were other more realistic models to be considered, they could easily be imported into the TLM mesh and be the basis of the simulation.

In the scope of our study, we shall use Elfouhaily's spectrum to render sea patches of relatively small size. The reason for this is the consequent computation time involved by a large TLM zone. The idea is therefore to operate the TLM calculations over a small sea patch, though large enough to account for the phenomena responsible for the backscattering of the electromagnetic wave by the sea surface. As already stated, the physics of the phenomenon state that most of the backscattering will be the effect of surface waves of comparable size to the incident electromagnetic wavelength. Therefore, considering the minimum wavelength λ_{min} in the emitted spectrum, performing the calculation over a zone of dimensions a few λ_{min} will be ideally suited. Note that, in the context of the yielding of a global nRCS over a large area of sea, it would also be necessary that waves larger than the patch be taken into account in order to consider variations of the global incident angle over the patch. This issue shall be addressed in section III-D.

Figure 3 shows a realisation example of a sea surface generated through the means of Elfouhaily's spectrum for a wind speed of 5 m.s^{-1}. The wind propagates upwards on the figure, and the surface was first generated on a 3 km-wide zone to encompass the whole wave spectrum before being reduced to a 300 m-wide patch for a better visibility of details.

B. Practical implementation

As Elfouhaily's spectrum can be numerically converted into a discrete elevation matrix (using a simple 2-D discrete inverse Fourier transform), it is straight-forward to obtain a numerical surface to import into the TLM mesh. Ideally, the modelled interface should separate two blocks of TLM nodes, one affected with air propagation coefficients, and the other with water characteristics. Indeed, this type of representation is

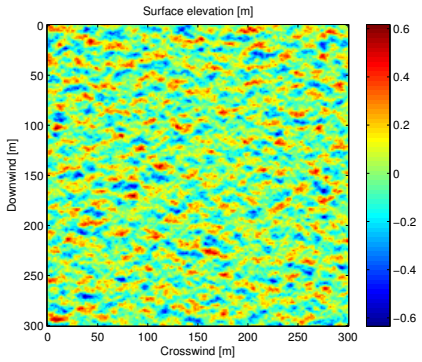

Figure 3. Illustration of a sea surface of side 300 m generated through the use of Elfouhaily's spectrum; wind speed is 5 m.s^{-1} and wind is directed vertically.

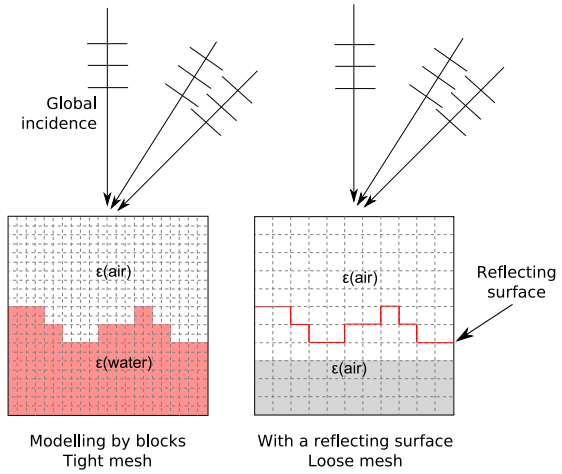

Figure 4. Illustration of the two modelling possibilities compared: left, the "block" configuration, with the sea zone defined with salty water electromagnetic characteristics; right, the "surface" configuration, where all cells have air characteristics, leading to a much more practical meshing step.

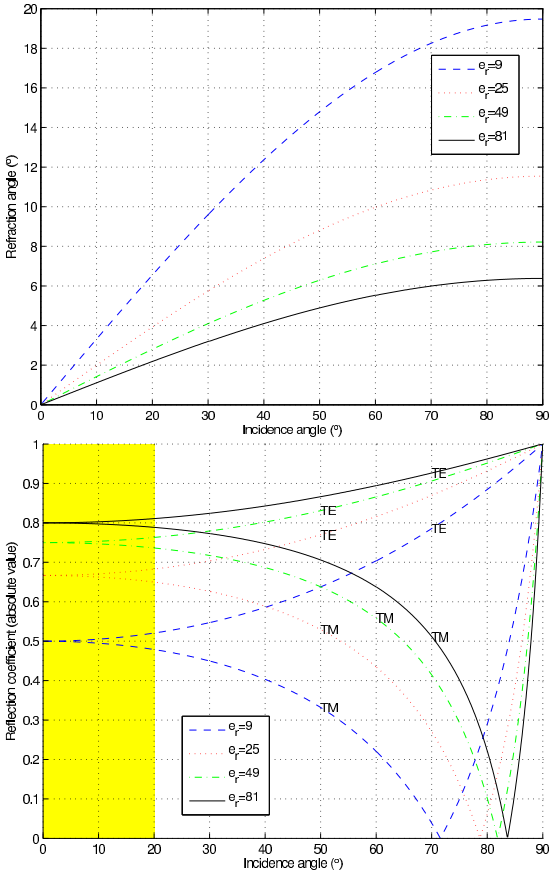

Figure 5. Behaviour of the refraction angle depending on the incidence angle and the relative permittivity of the refractive medium (top), and dependence of the reflection coefficient of the TLM cell as a function of the incident angle (bottom); the coloured zone displays the zone of interest where the reflection coefficient can be taken as constant, for both transverse electric and magnetic modes.

cumbersome, since the limiting condition on the spatial mesh size changes to $\frac{\lambda_{min}}{10\sqrt{\varepsilon_{max}}}$ if the propagation occurs in a medium different from air, ε_{max} being the maximal electric permittivity encountered. In the case of water, for radar waves, we can expect a $\frac{\lambda_{min}}{80}$ factor [26]. Computation times are increased accordingly. Arguing that the penetration of electromagnetic waves into water is very shallow at radar frequency, we propose to change the model and to use the synthesised sea surface as a mere interface: it shall separate two blocks of "air" characteristics, and will represent an electromagnetic frontier, whilst being given a reflection factor depending on the wavelength.

This is illustrated on Fig . 4. One shall note that the shaded cells on the sketch can be omitted from the simulation scheme, reducing the computation domain and thus the calculation time. The reflection factor we choose to allocate to each micro-facet constituting the electromagnetic frontier is taken as that of a planar water surface with normal incidence. For a water domain free of sources and with a limited roughness, on average, facets will be seen under an angle equal to that of the illumination. Rigorously speaking, the reflection factor should take the global incidence angle into consideration. However, given the fact that the salty water permittivity is very high (several dozens), the refraction angle into the water can be taken as very close to normal. As a result, the impedance of the watery domain will be seen as a constant, with a weak dependence on the incidence angle.

Fig. 5 provides with an illustration of this matter of fact: the refracted angles are calculated on the basis of the incidence angles and taking into account a given permittivity factor between the two media considered. Snell's law is simply used, with the refractive index value $n = \sqrt{\epsilon_r}$. It is found that the higher the permittivity contrast, the closer the refracted angle to the normal, with a value of as little as a few degrees for large permittivity differences and moderate incidence angles. Likewise, the second graph in Fig. 5 shows that reflection factors are practically constant for small incidence angles.

Thus, the expression of the reflection factor of any micro-facet constituting the surface will be considered independent of the global incidence angle, and its expression is simplified

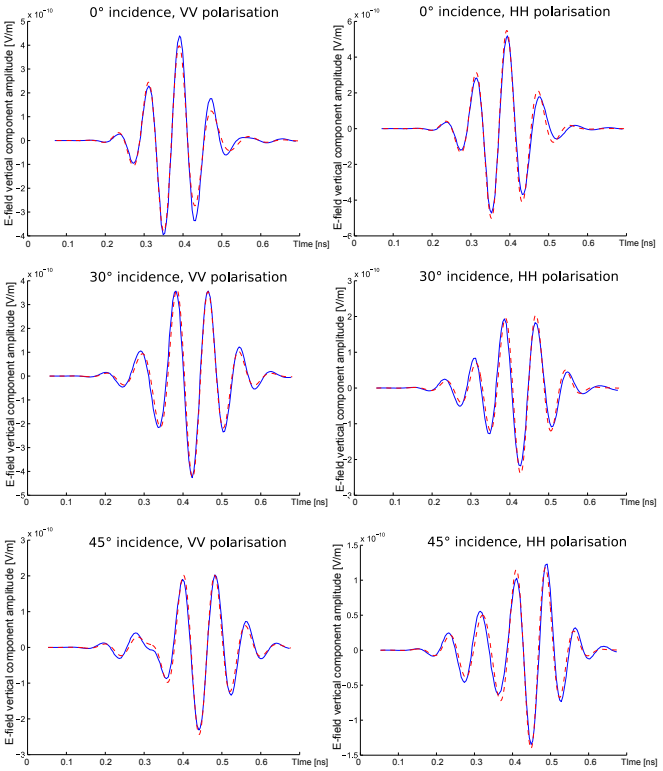

Figure 6. Simulated electric field back at the emission point showing the equivalence between block configuration (dotted line) and the use of an electromagnetic frontier (plain line), for a high permittivity contrast between air and water.

to [26]:

$$R = \frac{1-\sqrt{C}}{1+\sqrt{C}} \tag{1}$$

with, in vertical polarisation:

$$C_V = \frac{1}{\eta} \tag{2}$$

and in horizontal polarisation:

$$C_H = \eta \tag{3}$$

with $\eta = \varepsilon - i60\sigma\lambda$ the complex permittivity, where ε is the electric permittivity, σ the magnetic permeability and λ the electromagnetic wavelength. The complex permittivity can be evaluated using Debye's empirical formula [27].

Fig. 6 shows the accordance obtained for various conditions of simulation. A rough surface of size 0.1 m $\times$ 0.1 m was generated, and modelled twice, by first using a block approach (fine mesh of side 70 nodes) and then utilising an electromagnetic frontier (coarse mesh of side 10 nodes), following the principle illustrated on Fig. 4. Radar propagation over this surface was simulated with a 12-GHz carrier frequency modulated by a Gaussian of standard deviation 0.3 ns. The radar-surface distance was set to 3000 m and three different incidence angles were explored.

One can conclude that the agreement between the two methods is fairly verified for a high permittivity contrast and moderate incidence angles. Given the fact that the loose mesh approach computation was completed within 9 seconds versus 22 minutes for the fine mesh technique, we retained the former for the rest of the study.

After having exposed the practical implementation of our simulation method, we segue into more applied sections detailing the radar cross section calculation.

C. Calculation of nRCS over the illuminated patch

We shall here present the basic idea to derive a radar cross section, which stems quite simply from power considerations over the emitted and backscattered signals.

In a radar propagation, the so-called radar equation links the emitted and received powers P_t and P_r and reads in the monostatic case:

$$P_r = P_t G \frac{1}{4\pi R^2} \sigma \frac{1}{4\pi R^2} A_e \tag{4}$$

where G is the antenna gain, R is the radar-target distance, and A_e the effective aperture of the antenna. σ is the radar cross section (RCS) expressed in square metres.

By truncating the radar equation, and now considering the power surface densities S_t and S_r, one can re-write the expression of the RCS as [28]:

$$\sigma = 4\pi R^2 \left(\frac{S_r}{S_i}\right) \tag{5}$$

S_i and S_r are both expressed in Watts per square metre. The former is easily deduced from the emitted power P_t (in Watts) and the distance to the sea surface (in metres); the latter is issued from the output of the TLM simulation taken back at the source point.

The *normalised radar cross-section* (nRCS) σ_0 is defined as the ratio between the previously derived RCS σ and the illuminated area A_{ill}.

$$\sigma_0 = 4\pi \frac{R^2}{A_{ill}} \left(\frac{S_r}{S_i}\right) \tag{6}$$

where A is the illuminated area.

D. Considerations over the patch size

The previous paragraph addressed the computation of the nRCS on a small patch of sea water. Due to computation time restrictions, it is cumbersome to operate on a large area of the ocean. For this reason, it is for the moment not possible to directly compute the nRCS of a large patch of sea, i.e. including all wavelengths in the sea-surface spectrum. As a result, for any comparison with real, in-situ measurements of nRCS (radars usually operate on hecto- or kilometric-size swathes), we need to rely on a two-scale model. The operation is achievable through statistical means, though not detailed in the present paper.

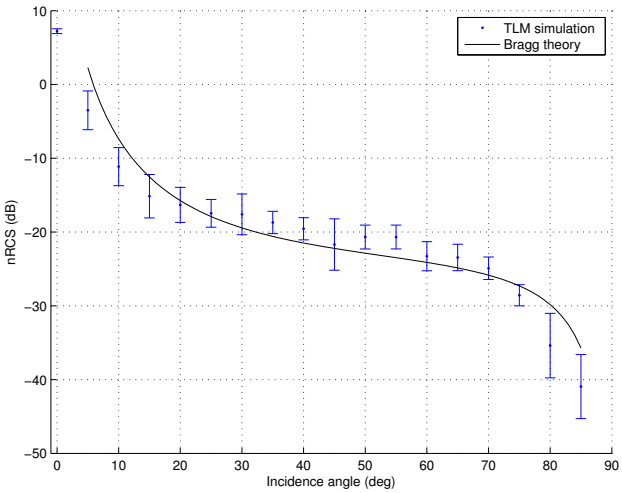

Figure 7. Angular dependence of the nRCS over a small sea patch, as simulated by the use of the TLM method, and comparison with Bragg scattering theory.

IV. Results

A. nRCS computation

Following the method exposed in III-C, one can evaluate the normalised radar cross section of a small sea patch. Because any rendition of the sea surface imported into the TLM mesh is eventually deterministic, it is necessary to perform a Monte-Carlo draw over several surface renditions, in order to yield an average nRCS.

Fig. 7 displays the angular dependence of the nRCS calculated over a small sea patch (side length of 7-λ with $f_0 = 3$ GHz) through the use of the TLM technique. The sea surface was generated using Elfouhaily's spectrum with a wind speed of 7.2 m.s^{-1} at a height of 10 m. Bell-shaped Huygens and Kirchhoff surfaces were used in order to obtain a more thorough response at grazing angles. For each angle, a Monte-Carlo draw over 50 renditions of the sea surface was performed. Crosses are the averages of the Monte-Carlo processes, and the error bars stand for the standard deviations over the calculated nRCS. The plain line is the theoretical Bragg scattering response of the surface.

We can notice a fairly good accordance between the simulation and the Bragg theory, especially at moderate incidence angles. For near-nadir incidence, the Bragg model diverges, which makes the comparison less opportune. As for grazing angles, a discrepancy is noted, along with large variations over the calculated nRCS, which points out some certain limits in our method.

B. SAR imaging simulation

Operating on a small patch of sea water, and repeating the process of illuminating the zone with an electromagnetic radar signal with different angles of incidence, one can simulate a SAR observation of the said patch, the image of which is eventually produced through the well-known technique of synthetic aperture.

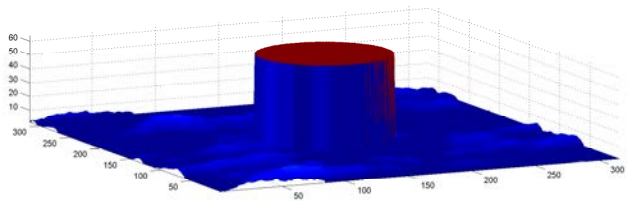

Figure 8. Illustration of an imported scene (metric size) within the TLM mesh in order to produce a SAR imaging simulation.

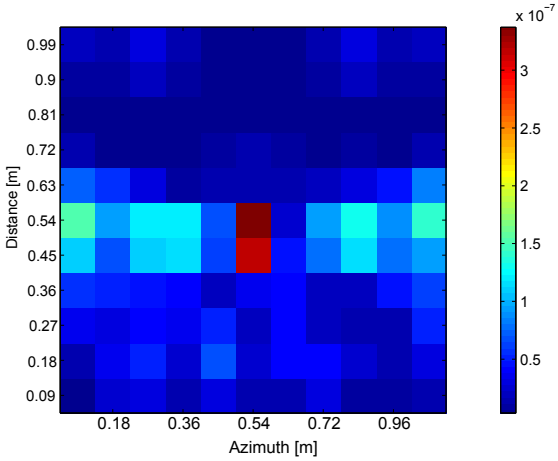

Figure 9. Simulated SAR image of the scene shown in Fig. 8. Amplitude scale: received signal amplitude, in V.m^{-1}.

Fig. 8 shows an example of a sea scene that can for instance be imported within the TLM mesh: we generated a sea surface of moderate roughness, in the midst of which a cylindrical, metallic object was added. One shall note that, due to the versatility of the method, any shape or any arbitrary electromagnetic characteristics can be affected to the object.

Fig. 9 is an overview of the type of simulated SAR image that can be obtained by combining several illuminations of the patch seen in Fig. 8 with different incidence angles, through the process of synthetic aperture. The simulation was carried out over a metric-size patch, with an impinging signal of carrier frequency 9.5 GHz (X-band), a minimum distance of 1000 m and an elevation incidence angle of 45°. The peak in the signal in the middle of the image is due to the specular response of the metallic cylinder.

V. Conclusion

In this paper, we have demonstrated the feasibility of the implementation of the Transmission-Line Matrix method in combination with ray-tracing to model the backscattering of a radar signal off the surface of the sea.

A direct application of such a tool is the estimation of normalised radar cross sections for small patches of sea of given geophysical constitution. An extension of these computations to large zones of sea can be performed. It is found that the calculated cross sections match fairly well theoretical models for small patches of sea; one can retrieve the radar

cross section evolution regarding the incidence angle. Another application of the method is the computation of SAR images of a small sea patch.

The advantage of the program developed is its great versatility: whereas in-situ measurements are often restricted to a certain number of incidence angles, fixed wind direction and radar frequency, etc., our method allows one to simulate virtually any set-up wanted, bearing in mind that some approximations are carried out. It is therefore an interesting tool to investigate the behaviour of radar waves when impinging the sea surface. Compared to other numerical methods, the TLM technique offers the opportunity to import objects over the sea surface, an option which is not topical with the Method of Moments for example.

The main drawback still to stand is the computation time required for the numerical method, but we can expect the times needed to be lowered with the use of up-to-date computational techniques, including parallelisation of the code. This would allow radar simulations over larger zones, broader frequency ranges, longer durations (possibility to simulate a whole chirp) and thus would widen the scope of the study. The direct simulation of observations over larger patches of sea could for instance be the basis for some SAR processing. Other upgrades to the method concern the use of variable meshing and inclusion of the dispersive effects. Finally, on-going work concerns the insertion of non homogeneous lossy media in PML for TLM computation. This should allow to limit the computational domain more accurately.

ACKNOWLEDGEMENTS

The basis to the coding of the TLM program was courtesy of Dr. Sandrick Le Maguer and Dr. Jérémy Lanoë from Telecom Bretagne's Microwave Department, to whom we are grateful.

REFERENCES

[1] A. G. Voronovich, *Wave Scattering from Rough Surfaces*. Berlin, Heidelberg, New York, Londres, Paris, Tokyo, Hong Kong, Barcelone, Budapest: Springer-Verlag, 1994.

[2] T. Elfouhaily and C.-A. Guérin, "A critical survey of approximate scattering wave theories from random rough surfaces," *Waves Random Media*, vol. 14, pp. R1–R40, Aug. 2004.

[3] N. Déchamps, N. de Beaucoudrey, C. Bourlier, and S. Toutain, "Fast numerical method for electromagnetic scattering by rough layered interfaces: Propagation-inside-layer expansion method," *Journal of the Optical Society of America A*, vol. 23, pp. 359–69, Feb. 2006.

[4] N. Pinel, C. Bourlier, and J. Saillard, "Bistatic radar cross section of two-dimensional random rough layers in the high-frequency limit," *EuRAD conference, Munich, Germany*, Oct. 2007.

[5] R. M. Axline and A. K. Fung, "Numerical computations of scattering from a perfectly conducting random surface," *IEEE Transactions on Antennas and Propagation*, vol. 26, pp. 482–488, 1978.

[6] A. K. Fung and M. F. Chen, "Numerical simulation of scattering from simple and composite random surfaces," *Journal of the Optical Society of America*, vol. 2, pp. 2274–2284, 1985.

[7] R. R. Lentz, "A numerical study of electromagnetic scattering from ocean-like surfaces," *Radio Science*, vol. 9, pp. 1139–1146, 1974.

[8] D. Maystre, "Electromagnetic scattering from perfectly conducting rough surfaces in the resonance region," *IEEE Transactions on Antennas and Propagation*, vol. 31, pp. 885–894, 1983.

[9] F. D. Hastings, J. B. Schneider, and S. L. Broschat, "A Monte-Carlo FDTD technique for rough surface scattering," *IEEE Transactions on Antennas and Propagation*, vol. 43, no. 11, pp. 1183–1191, Nov. 1995.

[10] C. H. Chan, S. H. Lou, L. Tsang, and J. A. Kong, "Electromagnetic scattering of waves by random rough surface: a finite-difference time-domain approach," *Microwave and Optical Technology Letters*, vol. 4, no. 9, pp. 355–359, Aug. 1991.

[11] A. K. Fung, M. R. Shah, and S. Tjuatja, "Numerical simulation of scattering from three-dimensional randmoly rough surfaces," *IEEE Transactions on Geoscience and Remote Sensing*, vol. 32, no. 5, pp. 986–994, Sept. 1994.

[12] J. Li, L.-X. Guo, and H. Zeng, "FDTD investigation on bistatic scattering from a target above two-layered rough surfaces using UPML absorbing condition," *Progress In Electromagnetics Research, PIER 88*, pp. 197–211, 2008.

[13] J. Li, L.-X. Guo, H. Zeng, and X.-B. Han, "Message-passing-interface-based parallel FDTD investigation on the EM scattering from a 1-D rough sea surface using uniaxial perfectly matched layer absorbing boundary," *Journal of the Optical Society of America*, vol. 26, no. 6, pp. 1494–1502, 2009.

[14] L.-X. Guo, J. Li, and H. Zeng, "Bistatic scattering from a three-dimensional object above a two-dimensional randomly rough surface modeled with the parallel FDTD approach," *Journal of the Optical Society of America*, vol. 26, no. 11, pp. 2383–2392, 2009.

[15] Y. Jihuan, Y. Yubo, X. Jingming, and G. Debiao, "Application of FDTD in EM scattering from rough surfaces," *5th international symposium on antennas, propagation and EM theory*, pp. 317–320, Aug. 2000.

[16] O. M. Ramahi, "Application of the complementary operator method to the finite-difference-time-domain solution of the three-dimensional radiation problem," *Microwave and optical technology letters*, vol. 9, no. 3, pp. 147–149, June 1995.

[17] T. Lurton, C. Sintès, and R. Garello, "Simulation of the radar observation of a sea patch using the TLM electromagnetic method," *IEEE Oceanic Engineering Society Newsletter*, no. 3, pp. 16–22, July 2009.

[18] J.-P. Bï¿½renger, "A perfectly matched layer for the absorption of electromagnetic waves," *Journal of Computational Physics*, vol. 114, no. 1, pp. 185–200, Oct. 1994.

[19] J. Lanoë, S. Le Maguer, and M. M. Ney, "A fractional derivative operator for surface impedance TLM modeling," *IEEE Microwaves and Wireless Component Letter*, vol. 17, no. 9, pp. 625–627, Sept. 2007.

[20] O. M. Phillips, *The dynamics of the Upper Ocean*, 2nd ed. Cambridge: Cambridge University Press, 1977.

[21] W. J. Pierson Jr and L. Moskowitz, "A proposed spectral form for fully developped wind seas based on the similarity theory of S. A. Kitaigorodskii," *Journal of Geophysical Research*, vol. 69, no. 24, pp. 5181–5190, 1964.

[22] K. Hasselmann, T. P. Barnett, E. Bouws, H. Carlson, D. E. Cartwright, K. Enke, J. A. Ewing, H. Gienapp, D. E. Hasselmann, P. Kruseman, A. Meerburg, P. Mueller, D. J. Olbers, K. Richter, W. Sell, and H. Walden, "Measurements of wind-wave growth and swell decay during the joint north sea wave project (JONSWAP)," *Deutsche Hydrographische Zeitschrift*, vol. Reihe A, no. 12, pp. 1–95, 1973.

[23] M. A. Donelan and W. J. P. Pierson, "Radar scattering and equilibrium ranges in wind-generated waves with application to scatterometry," *Journal of Geophysical Research*, vol. 92, pp. 4971–5029, 1987.

[24] V. Kudryavstev, V. Makin, and B. Chapron, "Coupled sea surface-atmosphere model : 2. spectrum of short wind waves," *Journal of Geophysical Research*, vol. 104, Apr. 1999.

[25] T. Elfouhaily, B. Chapron, K. Katsaros, and D. Vandermark, "A unified directional spectrum for long and short wind-driven waves," *Journal of Geophysical Research*, vol. 102, no. C7, pp. 15 781–15 796, July 1997.

[26] L. Boithias, *Propagation des ondes radioélectriques dans l'environnement terrestre*, 2nd ed. Paris: Dunod, 1984.

[27] P. Debye, *Polar Molecules*. New York: Reinhold Publishing Corp., 1929.

[28] C. Elachi and F. T. Ulaby, *Radar Polarimetry for Geoscience Applications*. Norwood, MA: Artech House, 1990.